

Sequence-dependent thermodynamics of a coarse-grained DNA model

Petr Šulc, Flavio Romano, Thomas E. Ouldridge, Lorenzo Rovigatti, Jonathan P. K. Doye, and Ard A. Louis

Citation: *The Journal of Chemical Physics* **137**, 135101 (2012); doi: 10.1063/1.4754132

View online: <http://dx.doi.org/10.1063/1.4754132>

View Table of Contents: <http://scitation.aip.org/content/aip/journal/jcp/137/13?ver=pdfcov>

Published by the [AIP Publishing](#)

Articles you may be interested in

[Introducing improved structural properties and salt dependence into a coarse-grained model of DNA](#)

J. Chem. Phys. **142**, 234901 (2015); 10.1063/1.4921957

[A coarse-grained model with implicit salt for RNAs: Predicting 3D structure, stability and salt effect](#)

J. Chem. Phys. **141**, 105102 (2014); 10.1063/1.4894752

[Coarse-grained modeling of DNA oligomer hybridization: Length, sequence, and salt effects](#)

J. Chem. Phys. **141**, 035102 (2014); 10.1063/1.4886336

[A coarse-grain three-site-per-nucleotide model for DNA with explicit ions](#)

J. Chem. Phys. **135**, 165104 (2011); 10.1063/1.3652956

[Residue energy and mobility in sequence to global structure and dynamics of a HIV-1 protease \(1DIFA\) by a coarse-grained Monte Carlo simulation](#)

J. Chem. Phys. **130**, 044906 (2009); 10.1063/1.3050106



NEW Special Topic Sections

NOW ONLINE
Lithium Niobate Properties and Applications:
Reviews of Emerging Trends

AIP | Applied Physics
Reviews

Sequence-dependent thermodynamics of a coarse-grained DNA model

Petr Šulc,¹ Flavio Romano,² Thomas E. Ouldridge,¹ Lorenzo Rovigatti,³
Jonathan P. K. Doye,² and Ard A. Louis¹¹*Rudolf Peierls Centre for Theoretical Physics, University of Oxford, 1 Keble Road, Oxford, OX1 3NP, United Kingdom*²*Physical and Theoretical Chemistry Laboratory, Department of Chemistry, University of Oxford, South Parks Road, Oxford, OX1 3QZ, United Kingdom*³*Dipartimento di Fisica, Sapienza–Università di Roma, Piazzale A. Moro 5, 00185 Roma, Italy*

(Received 15 July 2012; accepted 28 August 2012; published online 1 October 2012)

We introduce a sequence-dependent parametrization for a coarse-grained DNA model [T. E. Ouldridge, A. A. Louis, and J. P. K. Doye, *J. Chem. Phys.* **134**, 085101 (2011)] originally designed to reproduce the properties of DNA molecules with average sequences. The new parametrization introduces sequence-dependent stacking and base-pairing interaction strengths chosen to reproduce the melting temperatures of short duplexes. By developing a histogram reweighting technique, we are able to fit our parameters to the melting temperatures of thousands of sequences. To demonstrate the flexibility of the model, we study the effects of sequence on: (a) the heterogeneous stacking transition of single strands, (b) the tendency of a duplex to fray at its melting point, (c) the effects of stacking strength in the loop on the melting temperature of hairpins, (d) the force-extension properties of single strands, and (e) the structure of a kissing-loop complex. Where possible, we compare our results with experimental data and find a good agreement. A simulation code called oxDNA, implementing our model, is available as a free software. © 2012 American Institute of Physics. [<http://dx.doi.org/10.1063/1.4754132>]

I. INTRODUCTION

Living organisms store genetic information in DNA, a double-stranded polymer composed of a sugar-phosphate backbone with four different kinds of bases (adenine A, thymine T, cytosine C, or guanine G) attached. The bases have highly anisotropic mutual interactions that are responsible for the formation of non-trivial structures, such as helical double strands. To a first approximation, base-pairing occurs between complementary base pairs (A-T and G-C).¹ Given the reliability and programmability of base-pair formation, DNA is an obvious candidate for use in self-assembly. Indeed, DNA has been exploited as a building block for the assembly of nanostructures and active devices: successes include DNA computation,² motors,^{3,4} hierarchical self-assembly of tiles,⁵ and self-assembly of strands into large structures such as DNA origamis.⁶

Many theoretical and computational approaches have been developed to study DNA. At the most fine-grained level, quantum chemistry calculations can be used to study the interactions between nucleotides.^{7–12} While they provide valuable information about the ground state energies at a high level of detail, they are computationally demanding and do not allow for the study of dynamical processes involving breaking and forming of base pairs. Molecular simulation packages such as AMBER¹³ or CHARMM,¹⁴ that retain an all-atom representation of the nucleic acids but use empirical force fields to model their interactions, are extensively used for computational studies of both DNA and RNA as well as their interactions with proteins.¹⁵ Although faster than quantum chemistry methods, they still are computationally very demanding

and the time scales they can currently access are of the order of μ s, while many biologically and technologically relevant processes happen at the ms timescale or longer. At the moment, simulations of rare events such as the breaking of base pairs remain at the limit of what is possible. At the next level of complexity are coarser models of DNA^{16–30} that integrate out several degrees of freedom, such as replacing a group of atoms by a single site with effective interactions. While these models cannot describe the system at the same level of detail as atomistic simulations, they allow one to study much larger systems and address rare events. Finally, continuous models of DNA^{31–33} completely neglect the detailed chemical structure but allow for analytical treatment in the thermodynamic limit, and have been used to study macroscopic properties such as melting temperatures or properties of DNA under stress.^{32,33}

DNA nanotechnology exploits processes that include strand diffusion and the breaking and forming of base pairs. Computational methods describing such systems must be efficient enough to access the time scales at which these processes happen. Moreover, the coarse-grained model must be properly designed to capture the structural, thermodynamical, and mechanical properties of DNA in both the single- and double-stranded forms. Such a coarse-graining approach was recently used to develop the nucleotide-level model of Ouldridge *et al.*,^{34–36} that was subsequently successfully applied to the study of DNA nanotweezers,³⁴ kissing hairpins,³⁷ DNA walkers,³⁶ the nematic transition of dense solutions of short duplexes,³⁸ and the formation of DNA cruciforms.³⁹ The model was designed with an “average-base” representation that includes the specificity of base-pairing

but otherwise neglects the dependence of interactions on sequence. Consequently, the model is suited to study processes for which sequence heterogeneity is of secondary importance.

Nevertheless, many biological processes and technological applications of nucleic acids rely on sequence heterogeneity. It is well-known that A-T and G-C pairs have different relative binding strength,¹ with the latter being significantly stronger because of the presence of three rather than two interbase hydrogen bonds. Moreover, the stacking interactions that drive the coplanar alignment of neighboring bases are known to show significantly different behavior depending on sequence.¹ Furthermore, a strand of DNA possesses directionality, e.g., the phosphates of the backbone connect to the 3' and 5' carbon atoms in the sugars. Interactions within a strand are therefore distinct when the bases are permuted: for example, the interaction of neighboring A and T bases depends on whether the A is in the 5' direction with respect to the T or *vice versa*. Besides thermodynamic properties, it has been observed that mechanical and structural properties such as flexibility, helical twist, and even helix type are also influenced by the sequence.^{40–43}

To highlight the effects of sequence on the thermodynamics of DNA, we point out that the melting temperature of two oligomers with the same length but different sequences can vary by more than 50 °C, as shown in Fig. 1(a) where we compare the melting temperatures of poly(dA):poly(dT), poly(dG):poly(dC), poly(dCdG):poly(dGdC), and poly(dAdT):poly(dTdA)⁴⁴ sequences of various lengths at an equal strand concentration of 3.36×10^{-4} M. These melting temperature differences are only marginally diminished with increasing length and are exploited *in vivo*, where, for example, it has been observed that initiation sites of transcription are often composed of a higher than average number of A-T pairs.⁴⁵

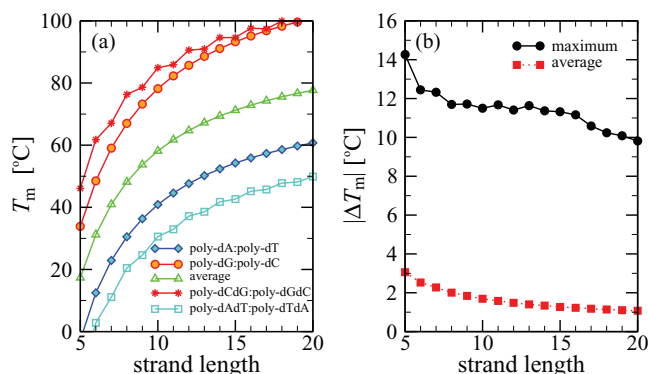


FIG. 1. (a) Melting temperatures versus duplex length as predicted by SantaLucia's nearest neighbor model⁴⁷ for a duplex consisting of poly(dA):poly(dT), poly(dAdT):poly(dTdA), poly(dC):poly(dG), or poly(dCdG):poly(dGdC) and an average sequence. (b) Maximum (circles) and average (squares) difference in melting temperature for strands with nucleotide positions randomly permuted. The terminal base pairs are kept the same, thus neutralizing different end effects. Data were generated by selecting 50 000 random sequences at each length and permuting each 5000 times. The differences show the importance of the order of the nucleotides in the sequence.

Note that beside the number of A-T and G-C base pairs, the actual order of nucleotides in the sequence is also important: two sequences of the same length and the same number of A-T and G-C base pairs can still have melting temperatures that differ by more than 10 °C, as shown in Fig. 1(b).

Given these large variations, it is important to have a model that captures at least the thermodynamic effects of sequence. We note that some of the other coarse-grained models of DNA that have been developed do include sequence effects in various level of detail, including sequence dependent base-pairing interactions¹⁶ and also sequence-dependent stacking¹⁷ and cross-stacking interactions.¹⁸ An extension⁴⁶ of the model in Ref. 16 also has base pair deformability parametrized to the values determined by analysis of DNA-protein crystal complexes.⁴¹ In contrast to these models, the model presented in Refs. 34–36 was specifically developed for applications in DNA nanotechnology and was primarily designed to represent the single- to double-stranded transition in a sufficiently physical manner. The aim of this work is to introduce a parametrization of this model that captures the sequence-dependence of DNA thermodynamics and to use it to study sequence effects on simple test systems.

We first present the original coarse-grained DNA model of Ouldridge *et al.*^{34–36} and then describe the fitting procedure we developed for the sequence-dependent interactions. We test the parametrization on melting of duplexes and hairpins, the latter being a case to which the model was not fitted. We then explore the flexibility of the model by studying: (a) the heterogeneous stacking transition of single strands, (b) the tendency of a duplex to fray at its melting point, (c) the effect of stacking strength in the loop on the melting temperature of hairpins, (d) the force-extension properties of single strands, and (e) the structure of a kissing-loop complex.

II. AVERAGE BASE COARSE-GRAINED DNA MODEL

The coarse-grained DNA model, on which this work is based, is described in detail in Refs. 35 and 36. It represents DNA as a string of nucleotides, where each nucleotide (sugar, phosphate, and base group) is a rigid body with interaction sites for backbone, stacking, and hydrogen-bonding interactions. The potential energy of the system is

$$V_0 = \sum_{(ij)} (V_{b.b.} + V_{stack} + V'_{exc}) + \sum_{i, j \neq (ij)} (V_{HB} + V_{cr.st.} + V_{exc} + V_{cx.st.}), \quad (1)$$

where the first sum is taken over all nucleotides that are nearest neighbors on the same strand and the second sum comprises all remaining pairs. The interactions between nucleotides are schematically shown in the Fig. 2, and the explicit forms can be found in Refs. 35 and 36. The hydrogen bonding (V_{HB}), cross stacking ($V_{cr.st.}$), coaxial stacking ($V_{cx.st.}$), and stacking interactions (V_{stack}) explicitly depend on the relative orientations of the nucleotides as well as on the distance between interaction sites. The backbone potential $V_{b.b.}$ is an isotropic spring that imposes a finite maximum distance between neighbors, mimicking the covalent bonds

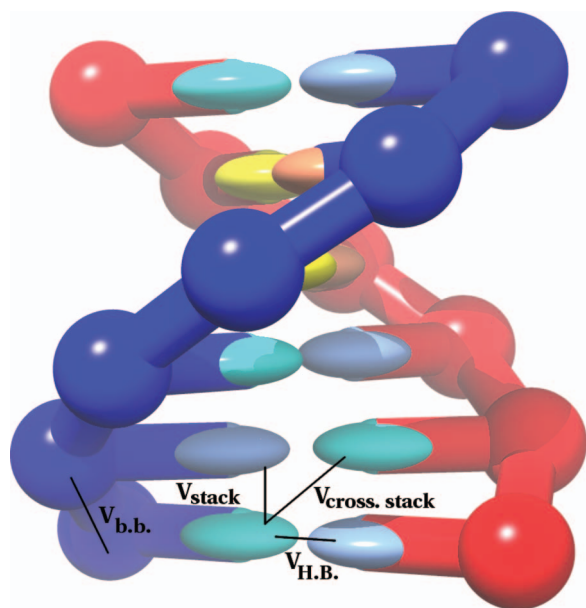


FIG. 2. The figure shows schematically the interactions between nucleotides in the coarse-grained DNA model for two strands in a duplex. All nucleotides also interact with a repulsive excluded volume interactions. The coaxial stacking interaction is not shown.

along the strand. The coaxial stacking term, not shown in Fig. 2, is designed to capture stacking interactions between non-neighboring bases, usually on different strands. All interaction sites also have isotropic excluded volume interactions V_{exc} or V'_{exc} .

The coarse-grained DNA model of Refs. 35 and 36 was derived in a “top-down” fashion, i.e., by choosing a physically motivated functional form, and then focusing on correctly reproducing the free energy differences between different states of the system, as opposed to a “bottom-up” approach that starts from a more detailed representation of DNA and typically focuses on the accurate representation of local structural details. The interactions were originally fitted to reproduce melting temperatures of “average” oligonucleotides, obtained by averaging over the parameters of SantaLucia’s model.⁴⁷ In addition, the model is fitted to reproduce the structural and mechanical properties of double- and single-stranded DNA such as the persistence length and the twist modulus. The model allows for base pairing only between Watson-Crick complementary bases, but otherwise does not distinguish between bases in terms of interaction strengths.

The model was fitted to reproduce DNA behavior at a salt concentration ($[\text{Na}^+] = 0.5 \text{ M}$), where the electrostatic properties are strongly screened, and it may be reasonable to incorporate them into a short-ranged excluded volume. Such high salt concentrations are typically used in DNA nanotechnology applications, hence motivating this approach. It should be noted that the model neglects several features of the DNA structure and interactions due to the high level of coarse-graining. Specifically, the double helix in the model is symmetrical rather than the grooves between the backbone sites along the helix having different sizes, and all four nucleotides have the same structure.

The main purpose of this paper is to go beyond the average sequence parametrization by introducing sequence-dependent interaction strengths into the model.

III. PARAMETRIZATION OF SEQUENCE-DEPENDENT INTERACTIONS

We choose to perform a thermodynamic parametrization of the sequence-dependent interactions, aiming to reproduce melting temperatures of short DNA duplexes. We seek the parameters that best reproduce the melting temperatures as predicted by SantaLucia’s model,⁴⁷ which we treat as an accurate fit to experimental data on the melting of duplexes of different length and sequence. We restrict sequence dependence to the strength of the base pairing and stacking interaction terms, keeping all other parameters fixed to the values of the original fit.

A. SantaLucia’s nearest-neighbor model

In an important series of papers, SantaLucia^{47,48} summarized the results of multiple melting temperatures of DNA oligomers, and also presented a nearest-neighbor model that reproduces the results of melting experiments (hereafter referred to as the SL model). This popular model is the basis of a number of widely used oligomer secondary structure and melting temperature prediction tools.^{49–52} The model assumes that DNA can exist in two states, either single-stranded or in duplex form, and gives a standard free-energy change of formation $\Delta G(T)$ of the duplex with respect to the single strands as a function of temperature. The expected yields of duplexes can then be calculated as a function of temperature through the relation

$$\frac{[AB]}{[A][B]} = \exp(-\Delta G(T)/RT), \quad (2)$$

where $[A]$ and $[B]$ are molar concentrations of single strands, $[AB]$ is the molar concentration of the duplex, and R is the molar gas constant. This result assumes the system is dilute enough to behave ideally apart from associations, a condition fulfilled in the vast majority of experiments.

The SL model assumes that $\Delta G(T)$ is a sum of contributions, one for each base-pair step formed in a duplex with respect to the single-stranded state, along with corrections for end effects. A base-pair step consists of four bases; for example, the base-pair step GT/AC stands for a section of duplex that has GT bases on one strand and AC on the complementary strand. The SL model has 10 unique base-pair nucleotide steps: AA/TT, AT/AT, TA/TA, GC/GC, CG/CG, GG/CC, GA/TC, AG/CT, TG/CA, GT/AC, where pairs are given in 3′–5′ order along the strands.

The contribution to $\Delta G(T)$ of each term is divided into a temperature-independent enthalpy and entropy, so that the overall form of $\Delta G(T)$ is given by

$$\Delta G(T) = \Delta H - T\Delta S, \quad (3)$$

with ΔH and ΔS being the (temperature-independent) sum of the individual contributions to the enthalpy and entropy respectively. The SL model is a *two-state* model, in that it

considers two regions of state space (the duplex and single-stranded states) and assumes that there is a constant enthalpy and entropy difference between the two. In other words, it neglects the variation in enthalpy within the bound and unbound sub-ensembles.

The melting temperature T_m for a given sequence is defined in the SL model as the temperature at which half of the strands in the system are in the duplex state and the other half are in the denatured state. Using this definition, the SL model has an average absolute deviation of 1.6 °C when compared to known experimental melting temperatures of 246 duplexes with lengths between 4 and 16 base pairs.⁴⁸ We fit to the T_m as predicted by the SL model, rather than having to re-analyse the original experimental data. This choice allows us to fit to a large ensemble of different sequences whose melting temperatures we estimate using the SL model.

We emphasize that, in contrast to the SL model, our model itself does not exhibit ideal two-state behavior. Although we observe a large difference in the typical energies of single-stranded and duplex states, allowing us to clearly differentiate the two, we also observe significant variation within these sub-ensembles. Both single-stranded and duplex states have multiple microscopic degrees of freedom, which respond differently to changes in temperature. For instance, we observe fraying of duplexes (Sec. V B) and that the single strands undergo a stacking transition (Sec. V A). The net effect is that the ΔH and ΔS of transitions that would be inferred from our model are not temperature independent, unlike in the SL model.

Since the early works^{53,54} on DNA melting, different models of DNA thermodynamics have been developed. It is thus important to note that other approaches, capable of predicting DNA melting temperatures apart from the SL model, exist; in particular, the Poland-Scheraga model,⁵⁵ which describes the strands at the secondary structure level, consisting of helical regions and loops. A variant of this model has been recently developed in Ref. 56 and compared with available melting data for both short and long DNA strands. The model described in Ref. 57 was developed to predict the base-pair opening probability in a DNA duplex. It is based on sequence-dependent thermodynamic parameters that have been shown to provide quantitative agreement with studies of the dynamics of DNA bubbles.^{57–59} Finally, the recently developed nearest-neighbor model of Ref. 60 uses the mechanical unzipping of DNA hairpins to infer the individual base pair step free energies that can then be used for estimating melting temperatures.

Since our parametrization procedure only requires estimates of the melting temperature for a large set of DNA sequences, it could be also used to fit our model to the melting temperature predictions of different models than the SL model.

B. Fitting of the parameters

Our model was originally parametrized to reproduce the melting temperatures of average sequences as predicted by the SL model. Since the SL model is constructed on the level

TABLE I. Summary of the final parameters that were fitted to reproduce melting temperatures of randomly chosen oligonucleotides as predicted by the SL model. Base steps are in 3′–5′ direction.

Base pairing	α_{ij}
AT	0.8292
GC	1.1541
Stacking	η_{ij}
GC	1.027
CG	1.059
AT	0.947
TA	0.996
GG, CC	0.978
GA, TC	0.970
AG, CT	0.982
TG, CA	1.009
GT, AC	1.019
AA, TT	1.042

of base-pair steps, it cannot be used to differentiate between intrastrand interactions within a step: for example, AA and TT or AG and CT. We therefore set the stacking interaction strengths of bases that belong to the same base-pair step to be equal in our parametrization procedure.

To parametrize our coarse-grained DNA model's potential V_0 (Eq. (1)), we scale the V_{stack} and V_{HB} interaction terms by the factors α_{ij} and η_{ij} , respectively, i.e.,

$$V_{H.B.} \rightarrow \alpha_{ij} V_{H.B.}, \quad (4)$$

$$V_{\text{stack}} \rightarrow \eta_{ij} V_{\text{stack}}, \quad (5)$$

where α_{ij} and η_{ij} are constants for a given nucleotide pair ij . There are therefore 10 parameters η_{ij} (as shown in Table I) and two parameters α_{CG} and α_{AT} to fit. Making the cross-stacking interaction sequence-dependent would also influence melting temperatures, but as we will discuss later, sequence-dependent stacking and base-pairing interactions provide enough parameters to obtain results in almost complete agreement with the predictions given by the SL model. To fit the 12 coefficients η_{ij} and α_{ij} , we used a set \mathcal{S} of oligonucleotides of lengths 6, 8, 10, 12, and 18 for which we calculated the (salt-adjusted) melting temperatures using the SL model. The set contained 2000 randomly generated sequences for each of lengths 8, 10, 12, 18, and all 4160 sequences of length 6. The set was then reduced to contain only heterodimers, leaving 12 022 sequences in total. We chose to remove homodimers (self-complementary sequences) for convenience, because the inference of the bulk melting temperatures from simulations of the formation of a single duplex is different from that for heterodimers, as discussed in Ref. 61.

We select the parameter set that minimizes the function

$$f(\alpha_{ij}, \eta_{ij}) = \sum_{s \in \mathcal{S}} |T_m^s(\text{SL}) - T_m^s(\alpha_{ij}, \eta_{ij})|, \quad (6)$$

where $T_m^s(\text{SL})$ is the melting temperature of the oligonucleotide s in the set \mathcal{S} as predicted by the SL model and $T_m^s(\alpha_{ij}, \eta_{ij})$ is the melting temperature predicted by our model with sequence-dependent base pairing and stacking potentials

$\alpha_{ij} V_{\text{H.B.}}$ and $\eta_{ij} V_{\text{stack}}$. To accurately fit α_{ij} and η_{ij} , we hence need estimates of the melting temperatures of many different sequences for many different values of the interaction parameters.

If one simulates a system consisting of two complementary strands in the simulation box at exactly the melting temperature then the ratio of observed duplex states to single-stranded states

$$\Phi = \frac{N_{\text{duplex}}}{N_{\text{single}}} \quad (7)$$

should be equal to 2 for heterodimers and 1 for homodimers. The value of 2 for heterodimers is a correction for finite size effects that arise when one simulates only two strands instead of a bulk ensemble at the same average concentration.⁶¹ The correction assumes that the density of strands is low enough that they behave ideally apart from association.

To calculate melting temperatures for the large set of sequences \mathcal{S} , we employed a histogram reweighting method.^{62,63} We generated once, for each duplex length considered, a set of 5000 single-stranded and 10 000 duplex configurations $\mathcal{C}_{\text{single}}$ and $\mathcal{C}_{\text{duplex}}$. The configurations in $\mathcal{C}_{\text{single}}$ and $\mathcal{C}_{\text{duplex}}$ were sampled from the Boltzmann distribution of strands of sequence s_0 at the melting temperature T_0 using the average parametrization (i.e., $\alpha_{ij} = 1$ and $\eta_{ij} = 1$). Simulations were performed in a cell that gave a concentration of 3.36×10^{-4} M for each strand. Twice as many duplex as single-stranded states were sampled because they appear in exactly this ratio in a simulation of two strands at the melting temperature of a given sequence in the average model (T_0). Sampling was done at sufficiently large intervals that the configurations in $\mathcal{C}_{\text{single}}$ and $\mathcal{C}_{\text{duplex}}$ were uncorrelated.

In order to find the ratio $\Phi_s(T, \alpha_{ij}, \eta_{ij})$ for a sequence s at temperature T with a parameter set α_{ij} and η_{ij} that corresponds to a potential $V(\alpha_{ij}, \eta_{ij}, T)$, states in $\mathcal{C}_{\text{single}}$ and $\mathcal{C}_{\text{duplex}}$ were reweighted by the factor

$$w_{l,s}(T, \alpha_{ij}, \eta_{ij}) = \exp\left(\frac{V_0^{l,s_0}(T_0)}{k_B T_0} - \frac{V^{l,s}(\alpha_{ij}, \eta_{ij}, T)}{k_B T}\right), \quad (8)$$

where $V_0^{l,s_0}(T_0)$ is the energy of the l th state generated at temperature T_0 using the sequence s_0 in the average model, and $V^{l,s}(\alpha, \eta, T)$ is the sequence-dependent potential evaluated on the same l th state for the sequence s . Note that both interaction potentials are a function of temperature because the stacking interaction term in the model is temperature dependent.^{35,36} The configurations used in Eq. (8) are generated at T_0 with V_0 and s_0 , but each is counted with a weight that corresponds to the desired set of new parameters.

The ratio of the duplex to single-stranded states for a given temperature T and parameters α_{ij}, η_{ij} becomes

$$\Phi_s(T, \alpha_{ij}, \eta_{ij}) = \frac{\sum_{l \in \mathcal{C}_{\text{duplex}}} w_{l,s}(T, \alpha_{ij}, \eta_{ij})}{\sum_{k \in \mathcal{C}_{\text{single}}} w_{k,s}(T, \alpha_{ij}, \eta_{ij})}, \quad (9)$$

where the index l runs through all generated duplex states while k runs through all generated single stranded states. Using this method, $\Phi_s(T, \alpha_{ij}, \eta_{ij})$ can be generated for a set of temperatures and interpolated in order to find T such that

$\Phi_s(T, \alpha_{ij}, \eta_{ij}) = 2$, which is by definition the melting temperature T_m of a given duplex.

The histogram reweighting method assumes that the ensemble of configurations generated at temperature T_0 with potential V_0 for sequence s_0 is also representative of the state space of the system at temperature T and potential $V(\alpha, \eta, T)$ for sequence s . To check whether we included enough states, we compared the estimation of the melting temperature by histogram reweighting of 15 000 states to an estimation that only used 6000 different states. For a test case of 71 000 sequences of oligonucleotide lengths 8, 12, and 18, the mean absolute deviation of the difference between the predicted T_m was smaller than 0.1 °C, suggesting that the choice of 15 000 states provides a large enough ensemble for estimating the melting temperatures, at least on average.

To find a set of parameters that minimizes the function in Eq. (6), we ran a simulated annealing algorithm.⁶³ We first fitted the base-pairing strengths α_{CG} and α_{AT} while holding the stacking parameters constant. Then we fitted the 10 stacking parameters η_{ij} in a second step. The separate fitting of the two sets of parameters simplifies the fitting procedure, as the converged values for α_{ij} provide an initial point for the stacking parameters fitting. It also allows us to compare the performance of a model where only the base-pair interaction strengths are sequence-dependent to the one where both base-pairing and stacking interactions are sequence-dependent.

We note that our fitting procedure requires the ability to efficiently estimate melting temperatures. The histogram reweighting method, using the generated states, takes only about 1 s to calculate the melting temperature of a given sequence. This is a huge reduction in computer time as compared to umbrella sampling simulations,⁶⁴ which were used in the parametrization of the original average sequence model.³⁵ The umbrella sampling simulation samples multiple single-to double-stranded transitions for a given oligomer and requires around two weeks of computer time to calculate the melting temperature to within 0.3 °C accuracy for the sequence lengths that we considered for our parametrization. Thus, our histogram re-weighting methodology provides the crucial speed-up that made the parametrization possible.

C. Parametrization results

While the parameters α_{CG} and α_{AT} were fairly robust to details of the optimization procedure, the parameters η_{ij} were more sensitive. In order to uniquely determine these parameters, we selected the set with the smallest average error on an additional test set of 95 958 sequences that included all sequences of lengths 5, 6, 7, and 8 for which the SL model predicts a T_m greater than 0 °C for the concentration 3.36×10^{-4} M, plus a set of randomly generated sequences of lengths 10, 12, and 18. The final set of parameters η_{ij} and α_{ij} , as introduced in Eqs. (4) and (5), is shown in Table I.

Figure 3 compares a histogram of the difference

$$\Delta T_m = T_m(\alpha_{ij}, \eta_{ij}) - T_m(\text{SL}), \quad (10)$$

between the melting temperatures $T_m(\alpha_{ij}, \eta_{ij})$, calculated by our coarse-grained model (using histogram reweighting) and the $T_m(\text{SL})$ of the SL model, determined for each of the 95 958

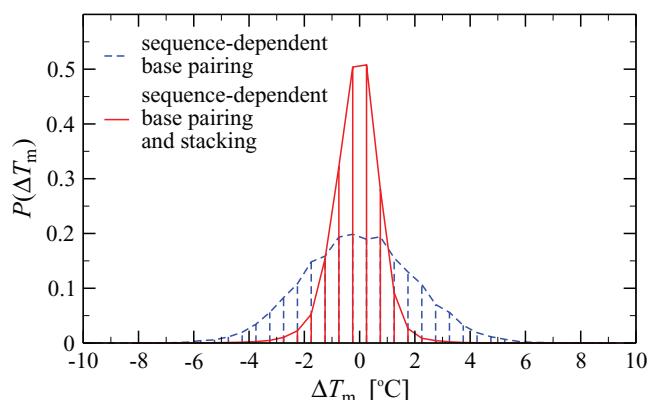


FIG. 3. The histogram shows the performance of the fitted DNA coarse-grained model for the set of 95 958 test sequences. ΔT_m is the difference between the melting temperature predicted by the coarse-grained model and by the SL model. The blue dashed curve corresponds to a model where only hydrogen-bonding interactions were parametrized and the red curve corresponds to the model where the stacking interactions are also sequence-dependent (using values from Table I).

sequences in our test set. The dashed curve shows our model's performance when only the base pairing interactions are sequence-dependent (parameters α_{CG} and α_{AT} from Table I) and the stacking parameters η_{ij} are all set to unity. The solid curve shows the histogram when the melting temperatures are calculated by our model with both hydrogen bonding and stacking sequence-dependent parameters. The standard deviation of the distribution of ΔT_m with sequence-dependent base pairing and average stacking is 2 °C, while the standard deviation for the case where stacking is also sequence-dependent is 0.85 °C. This compares to a standard deviation of 8.6 °C for the original average-base model. We note that although the average deviation is very small, there are a number of melting temperatures in our set that differ significantly more than one would expect from a Gaussian distribution with this standard deviation. These outliers are typically highly repetitive sequences.

Since the SL model has an average absolute deviation of 1.6 °C when compared to experimental melting temperatures of 246 duplexes of lengths between 4 and 16, there is little point in trying to further improve our predictions with respect to it. That it is possible to reproduce the predictions of the SL model with our set of 12 parameters also implies that it would not be appropriate to introduce sequence dependence for other terms in the interaction potential by fitting only to $T_m(\text{SL})$. Instead, other physical input would be needed.

It is also important to point out that, as discussed previously, by fitting to a model which considers only base pair steps it is not possible to distinguish between, for example, AA or TT stacking strengths, which are known to be different.⁶⁵ Even though we treat stacking within base pair steps equally, our method in principle allows the stacking interaction for each individual stacked pair to be parametrized differently. But in order to do this fitting, new experimental data are needed. We further discuss the parametrization of stacking interactions in Sec. V C.

IV. TESTS OF THE PARAMETRIZATION

In this section, we test the performance of our sequence-dependent parametrization by comparing the melting temperatures of selected duplexes, as well as for hairpins, to which the model was not directly fitted.

We have also tested the structural and mechanical properties of double-stranded DNA (away from thermodynamic transitions) on a randomly generated sequence with around 50% GC-content and confirmed that they are not changed with respect to those of the original average-base parametrization. So, our double-stranded persistence length remains approximately 125 base pairs, and the B-DNA structure produced by the model is the same as in Refs. 35 and 36. On the other hand, the structural and mechanical properties of single-stranded DNA properties do differ from those of the average model, and are studied in Secs. V A and V D.

A. Duplex melting

To further test our histogram reweighting method, we calculated several oligomer melting temperatures using umbrella sampling Monte Carlo simulations.⁶⁴ While the histogram reweighting method estimates the melting temperature using the same 15 000 generated states for each duplex length considered, and extrapolates from the average-base to the sequence-dependent potential, umbrella sampling simulations are run separately for each sequence considered. The umbrella sampling uses the sequence-dependent potential and is done close (within 3 °C) to the melting temperature of given sequence, hence providing a more accurate estimation of the melting temperatures in our model.

The comparison between the different methods are shown in Table II for a series of sequences. On average, the histogram reweighting and the umbrella sampling agree to within 0.3 °C, which is very satisfactory. However, there is one significant outlier, ATATAGCTATAT, for which a difference of 2.3 °C was obtained. One reason for the difference may be that the melting temperature is about 16.6 °C lower than the melting temperature of an average strand of the same length from which the configurations were taken for the histogram reweighting. This difference is larger than the typical

TABLE II. Duplex melting temperatures (shown in °C) as predicted by our coarse-grained DNA model using umbrella sampling Monte Carlo simulations ($T_m(\text{US})$) and histogram reweighting ($T_m(\text{HR})$) compared to that for the SL model ($T_m(\text{SL})$). $T_m(\text{SL-avg})$ is the melting temperature as predicted by the averaged SL model, which depends only on the length of the sequence. Sequences are specified in 3'–5' direction.

Sequence	$T_m(\text{US})$	$T_m(\text{HR})$	$T_m(\text{SL})$	$T_m(\text{SL-avg})$
AAGCGT	38.0	38.2	39.6	31.2
GAGATC	24.4	24.0	22.0	31.2
TCTCCATG	44.7	44.6	44.6	48.2
CCCGCCGC	71.1	70.6	71.1	48.2
ATTTATTA	21.2	21.3	23.9	48.2
ATATAGCTATAT	47.0	49.3	48.1	64.7
ATGCAGCTGCCG	74.0	74.3	72.6	64.7
GCGCAGCTGCCG	79.8	79.6	79.0	64.7

width of the melting transition (around 10 °C for sequences of length 12). Moreover, the sequence has a relatively high A-T content and may adopt structures with significant fraying at the ends that contribute to the ensemble of configurations for the actual strand. Such frayed states might have been poorly sampled when the ensemble was generated using the average base model. For these reasons, the sampled configurations may not provide a good representation of the true state-space of the system. Nevertheless, a number of other sequences tested here also have melting temperatures that differ significantly from the average sequence, without exhibiting such a large difference in the predicted melting temperatures between the two methods. Although it may be true that including a significantly larger set of states in the histogram reweighting method could reduce the errors in these outliers, we decided not to pursue this route further, given that the accuracy of the underlying SL model is not much different than our parametrization errors. Should a significantly more accurate model of the experimental data become available, however, then it may be that this point needs to be revisited.

B. Hairpin melting temperatures

We also tested our model's predictions for hairpin melting temperatures. This provides a distinct test of the parametrized model, since the sequence-dependent parameters were fitted to duplex melting temperatures only. Importantly, this test also probes the quality of the model's description of the single-stranded state, a feature often neglected in DNA models. We test melting temperatures of four different hairpin-forming sequences with different stem and loop lengths. We used strong and weak stem sequences to highlight sequence effects.

The simulations were performed with umbrella sampling using the number of correct base pairs in the stems as a reaction coordinate. The melting temperature T_m is defined as the temperature at which the system spends half of the time in the hairpin state, which is in turn defined as the ensemble of configurations with one or more correct base pairs. In Table III, we compare our predictions for T_m with those obtained from the SL model. The average-base parametrization was previously found to consistently underestimate T_m for hairpins by approximately 3 °C, but to show the correct variation with loop and stem length.³⁵ The sequence-dependent parametrization presented here also tends to underestimate T_m by roughly the same amount, but the sequence effects are well captured.

We further examine the effect of stacking on the melting temperature of hairpins with longer loops in Sec. V C, where

TABLE III. Hairpin melting temperatures (shown in °C) as predicted by our coarse-grained DNA model (T_m) compared to the prediction by the SL model $T_m(\text{SL})$. Sequences are specified in 3'-5' direction.

Sequence	T_m	$T_m(\text{SL})$
AGCGTCACGC - (T) ₆ - GCGTGACGCT	86.5	86.7
AGTATCAATC - (T) ₆ - GATTGATACT	62.2	64.4
AGCGTC - (T) ₁₀ - GACGCT	64.5	67.0
AGTATC - (T) ₁₀ - GATACT	44.0	47.3

we compare our model with the experimentally measured influence of sequence content of the loop on the hairpin melting temperature, an observation which is beyond the SL model.

V. SEQUENCE-DEPENDENT PHENOMENA

To demonstrate some of the strengths and weaknesses of our new model, we present, in this section, a series of studies of DNA systems for which sequence plays a non-trivial role. The results were obtained from either Monte Carlo or dynamical simulations of the model. The Monte Carlo algorithm used is a Virtual Move Monte Carlo algorithm⁶⁶ and the molecular dynamics simulations were performed using a Brownian dynamics algorithm⁶⁷ with the thermostat as described in Ref. 68.

A. Heterogeneous stacking transition of single strands

Our model strands undergo a broad stacking transition, i.e., a transition from a state with all or the majority of neighboring bases coplanarly aligned to a state with disrupted alignment, as a function of temperature.^{35,36} Such a transition is also generally accepted to occur for DNA, although there is not a clear consensus in the literature about many aspects of this transition.¹

To investigate the sequence dependence of stacking in our model, we ran Brownian dynamics simulations for a 14-base single strand with sequence GCGTCATACAGTGC (the same sequence as studied in Ref. 69) at a range of temperatures. We measured the probability that a neighbor pair stacks. Two bases are considered to be stacked if the magnitude of their stacking interaction energy is at least 6% of its maximal value. The choice of a cutoff is one of convenience; we have checked that doubling it does not measurably change the results. Even though the different stacking strengths do not vary from the average by more than 7%, the effects on the stacking probabilities are still quite significant. For example, as shown in Fig. 4(a), the difference between the strongest (GC) and the weakest (AT) stacking pairs is large enough that the midpoints of the transitions are separated by about 40 °C.

The structure of the single strands is also heterogeneous, consisting of unstacked and stacked regions of various lengths, as illustrated in Fig. 4(b). The stacked regions adopt a helical geometry, whereas the unstacked regions are more disordered.

The strands are also dynamically heterogeneous: over time the stacked and unstacked regions grow and shrink, while the average probability that a given neighboring pair of bases stack varies with temperature and position is measured in Figure 4(a). Mechanical and structural properties of the single strands are therefore heterogeneous both in space and in time.

While we are confident that the existence of significant temporal and spatial heterogeneity in single strands is a robust qualitative prediction of our model, given the paucity of experimental and theoretical data on the detailed stacking interactions between individual bases, many questions about the nature and time scales of these heterogeneities remain open.

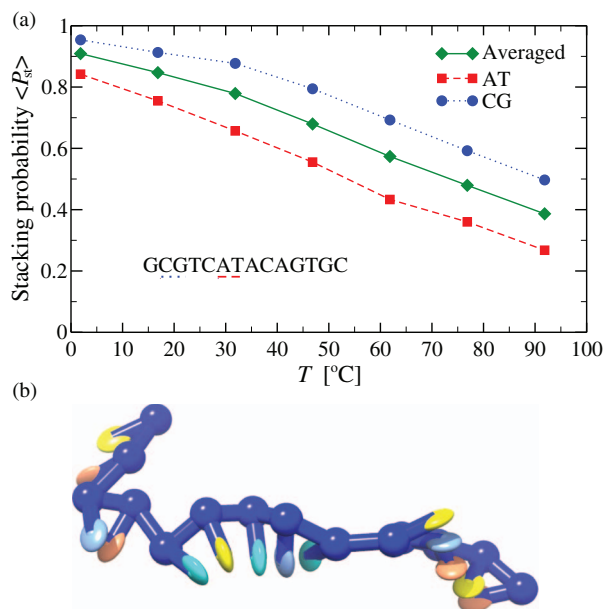


FIG. 4. (a) The stacking probability, calculated as the fraction of time in the stacked state, varies with temperature and is heterogeneous along the sequence. Circles correspond to the strongest stacking term, CG (underscored with dotted line in sequence), while squares correspond to the weakest stacking step, AT (underscored with a dashed line in the sequence). Diamonds correspond to the average of all the stacking along the sequence. (b) A typical single stranded configuration at 45 °C. The first two bases on the left are unstacked. The strand has three stacked regions, which adopt a helical geometry.

B. Hybridization free energy profiles of duplexes

For our average-base parametrization, we have previously seen that duplexes at their melting point typically have a terminal pair of bases that are unbound. This behavior is called fraying, and it is generally thought that the ease of fraying is sequence-dependent with A-T ends fraying more readily.⁷⁰ To explore the fraying behavior in our model, we study the free-energy profiles of the sequences ATATAGCTATAT, ATGCAGCTGCCG, and GCGCAGCTGCCG. Note that all three sequences have the same four central bases but different ends.

In Fig. 5, the free energies profiles are shown as a function of the number of the native base pairs formed between the complementary strands. The free energies were set to be equal to 0 in the state with 0 native base pairs, i.e., when the duplex is melted.

Of most interest is how the most stable duplex state depends on sequence. For the strand with two G-C ends, the free-energy minimum is a state with all 12 bonds formed, although the free-energy cost of opening up 1 base-pair is minimal. By contrast, for the case of either one or two A-T ends, the duplex has the lowest free energy in a state with 10 bonds formed. Although the system pays an energetic cost for having 2 bonds unformed, it gains entropy from this opening up of the end base pairs. Thus, our model strands exhibit fraying, with the expected stronger tendency to fray for duplexes with weaker A-T ends. Note that the sequence with two A-T ends frays despite being at a significantly lower temperature than the G-C rich sequence. Fraying has many consequences

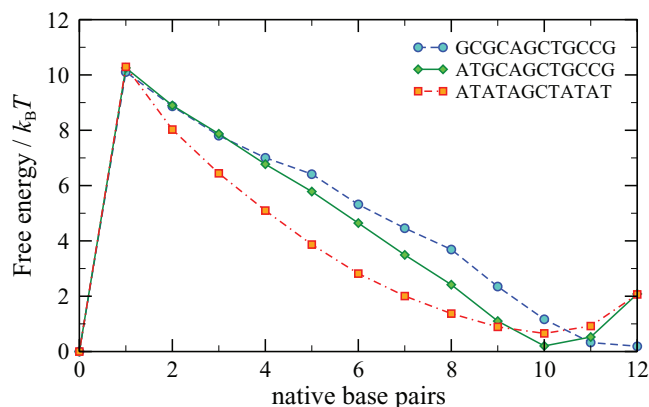


FIG. 5. Free energy profiles for three different duplexes of length 12 as a function of the number of complementary (native) base pairs of the two strands. The simulations for each duplex were run at their respective melting temperatures, namely 48 °C, 73 °C, and 80 °C.

for DNA behavior. For instance, it exposes the end bases, allowing them to take part in reactions with other strands, which is important, for example, in a toehold-free displacement process.⁷¹

Other features of note that are apparent from the free energy profiles in Fig. 5 are the nature of the first free energy jump and the shape of the minimum corresponding to the bound state. The fact that the first jump is almost the same for all three sequences reflects that it is dominated by the loss of center of mass entropy on association, which is the same (in units of $k_B T$) for the three systems. The shape of the free energy minimum corresponding to the duplex highlights differences in the ensemble of duplex states for different sequences. For the weakest sequence, at the melting point, the duplex can have as little as 7 base pairs for a significant fraction of the time, and roughly with the same probability as for it being fully closed. The most G-C rich sequence, on the other hand, shows little tendency to fray even at its melting point and it rarely breaks more than 3 base pairs.

C. Loop sequence effect on hairpin melting temperatures

In Sec. IV B, we tested our model on melting temperatures of hairpins with short loops of lengths 6 and 10. In the SL model, the loop contribution to the free energy difference for closing a hairpin is considered to be of purely entropic origin and sequence independent. However, it was observed experimentally⁷² that hairpins with the same loop lengths but different sequences have different melting temperatures. In particular, the experiment in Ref. 72 considers sequences with the same stem sequence and loops consisting of either poly(dA) or poly(dT). The observed difference in melting temperature of the two different loop sequences was 4 °C for loop length 12 and increased to 12 °C for loop length 30, with the poly(dA) loop always having lower melting temperature. It was proposed that the strand with a poly(dA) loop region has a higher rigidity in the single-stranded case due to the base stacking and thus pays a larger penalty for closing.

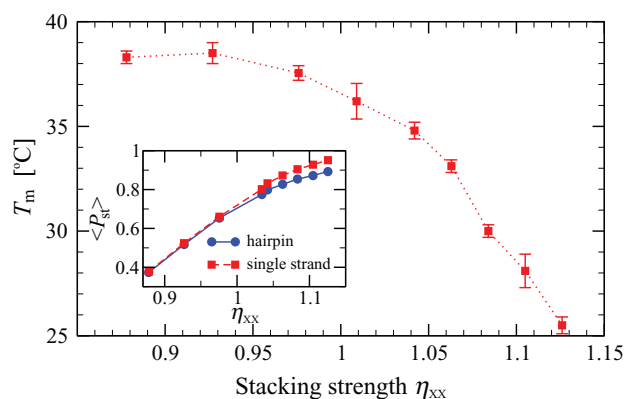


FIG. 6. Hairpin melting temperatures as predicted by our coarse-grained DNA model as a function of stacking strength within the loop. We use a sequence GGGTT-(X)₂₅-AACCC, where X is taken to stack as A with other bases, and with stacking strength η_{xx} with itself. The sequence is specified in 3′-5′ direction. The predicted melting temperature for the SL model is 37.8 °C. The inset shows stacking probability $\langle P_{st} \rangle$ within the loop region in the hairpin state (circles) and single-stranded case (squares) as a function of stacking strength η_{xx} .

Although the experiments in Ref. 72 were done at a salt concentration of 0.1 M, lower than the 0.5 M to which our model was fitted, it is instructive to see in general how stacking in the loop influences the stability of hairpins. We calculated the melting temperature for the sequences with the same stem sequence as in the experiment and a range of stacking strengths in the loop. Since our model does not distinguish between AA and TT stacking, we use an artificial base type X that is taken to stack as A with other bases and distinctly (with stacking strength η_{xx}) with other bases of the same type X .

The results, summarized in Fig. 6, show that for $\eta_{xx} \lesssim 1$, the melting temperatures are fairly insensitive to stacking strength whereas for $\eta_{xx} \gtrsim 1$, the melting temperature starts to drop significantly with increasing stacking strength. In the inset of Fig. 6, we show the average stacking probability in the loop, compared to that of the competing single-stranded state at the same temperature. In general, as the stacking strength increases, the probability that a piece of single-stranded DNA has long stacked regions also increases. The geometric constraints of the loop on stacking therefore become more pronounced with increasing strength, destabilizing the hairpin and leading to a drop in the melting temperature. On the other hand, for $\eta_{xx} \lesssim 1$, the stacked regions have an average length $\langle l \rangle \lesssim 3$, which is short enough that the hairpin geometry does not significantly affect the stacking.

If the data of Ref. 72 are to be interpreted using a model of stacking such as ours, we would infer that poly(dA) has a very high stacking probability at these temperatures, while poly(dT) has a significantly lower one. But, as the inset of Fig. 6 shows, we would not conclude that poly(dT) is necessarily largely unstacked.

It is interesting to note that the stacking strength where destabilization becomes noticeable coincides with the top end of our fitted strengths, and that if we were to separate poly(dT) and poly(dA) stacking strengths, it would not require an unreasonable change to give a signal of comparable size to that reported in Ref. 72. In particular, if one sets η_{AA} to 1.105

and accordingly adjusts η_{TT} to 0.979 in order to keep the average of the two coefficients the same as for our base-pair step parametrization, the obtained difference in melting temperature of the hairpins with poly(dA) and poly(dT) loop is about 9 °C. For these values of η_{TT} and η_{AA} , the standard deviation of melting predictions for the set of duplexes used in testing our parametrization increases by only 0.1 °C. Thus, if one wants to investigate a system where the difference in AA and TT stacking strengths plays an important role, these coefficients can be used. However, in the absence of a systematic study of the effects of loop sequence on hairpin melting temperature at high salt, we do not include differences between pairs that cannot be distinguished by the SL model in our parametrization in Table I.

D. Force-extension curves of single strands

The mechanical properties of single strands have been experimentally measured for both DNA and RNA^{60,65,73–77} to characterize their average as well as base-specific properties. In particular, qualitatively different behavior has been observed for single-stranded poly(dT) (poly(rU) in the case of RNA) compared to poly(dA) (poly(rC) or poly(rG) in the case of RNA); the latter exhibit significant deviations from standard polymer models such as freely-jointed and wormlike chains, whereas the former do not. These deviations—concave regions with negative curvature in the force-extension curves—are described as “plateaus.”^{65,73,75}

To investigate the effects of sequence on the mechanical properties of single strands in our model, we simulate mechanical pulling and obtain force-extension curves for 50-base strands at room temperature (25 °C). We consider polymers corresponding to our weakest and strongest stacking sequences, poly(dGdA) and poly(dA), which differ in η_{ij} by about 7%. We note that in Sec. V C, we used hairpin melting to distinguish AA and TT stacking strength, but the obtained values are open to enough uncertainty that in this section we return to our original parametrization. Our focus here is on the qualitative effect of stacking differences, rather than their quantitative values.

Figure 7(a) shows force-extension curves for our strongest and weakest stacking sequences. The concave section for strongly-stacked poly(dA) between 15 and 25 pN is qualitatively similar to the plateau-like features observed in experiment.^{65,73,75} The relatively weakly-stacked strand, poly(dAdG), follows a convex force-extension curve, which is fairly typical of a classical homo-polymer model.

The poly(dAdG) curve is similar to the one found for the average base model, which in turn is in reasonable quantitative agreement with experimental results for typical sequences. Although quantitative comparison with experimental data for non-homopolymeric sequences, such as λ -phage ssDNA,⁷⁷ is hampered by the presence of metastable secondary structure,^{76,78,79} at tensions above about 15 pN, where hairpins are disrupted, the extension per base at given force in the average model is within 10% agreement with Ref. 77. A detailed discussion of the agreement between the average model and experiment is given in Ref. 36.

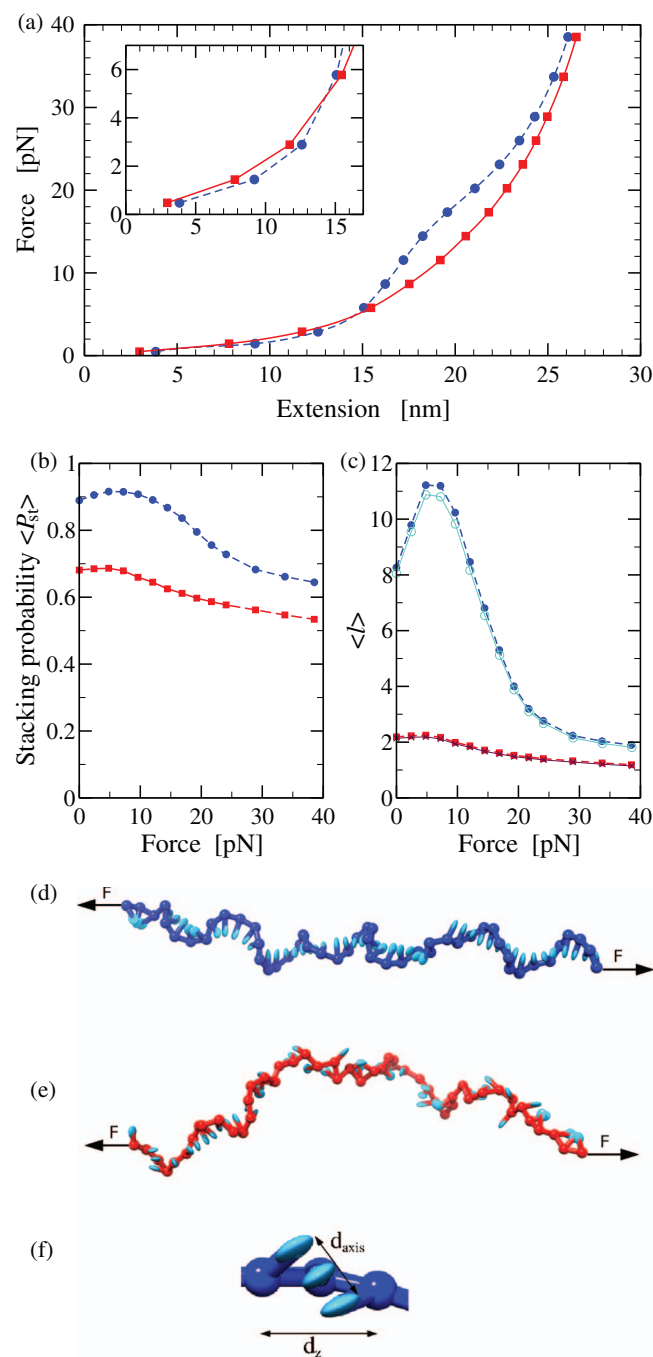


FIG. 7. (a) Extension of 50-nucleotide single-stranded DNA at 25 °C as a function of applied force. In all panels, blue circles correspond to a poly(dA) sequence (strongest stacking in our model), while red squares correspond to a poly(dGdA) sequence (weakest stacking). The inset in (a) shows a magnified section of the force-extension curve for low forces. (b) Stacking probability of a neighbor pair as a function of the applied force F . (c) Average length of a stacked domain $\langle l \rangle$ as a function of applied force F . The open circles and crosses show $\langle l \rangle_{\text{uncoop}}$ as predicted by the uncooperative stacking model (Eq. (11)) using $\langle P_{st} \rangle$ as measured for poly(dA) and poly(dGdA), respectively. (d) Visualization of a 50-base long poly(dA) ssDNA under a tension $F = 15$ pN, showing multiple stacked regions with helical geometry. The arrows indicate the applied force on the first and the last base. (e) Poly(dGdA) strand under a tension of 15 pN, consisting of short stacked regions as well as unstacked ones. (f) Magnified section of ssDNA illustrates that three stacked bases can align with the applied force without disrupting the stacking interaction. The contour length d_z , aligned with the force, is larger than the axial rise d_{axis} .

To understand the difference between the two single strands in our simulations, it is instructive to first recall that the strands consist of dynamically changing stacked and unstacked regions, as discussed in Sec. V A. When no force is applied, an unstacked region typically has a shorter end-to-end distance than a stacked region because it is more flexible and hence behaves more like a random coil. On the other hand, unstacked regions also have a greater maximum extension because the backbone is not restricted to a helical geometry as in the case of stacked regions.

To explore the effect of pulling the structure of the single strands, we measured the stacking probability $\langle P_{st} \rangle$ and the average length $\langle l \rangle$ of contiguously stacked sections for both strands, where a section of length l consists of $l + 1$ bases. The results, as a function of applied force, are plotted in Figs. 7(b) and 7(c). When no force is applied, the stronger-stacking strand poly(dA) has $\langle l \rangle \cong 8$ while the weaker-stacking strand poly(dAdG) consists mostly of short stacked regions with average length $\langle l \rangle \cong 2$.

As shown in the inset of Fig. 7(a), at low forces the stronger-stacking poly(dA) strand is more extensible than the weaker stacking one, by as much as 20% at 1 pN force. The reason for this difference is that long stacked sections have a smaller entropic cost for aligning with the applied force than unstacked regions do. However, as the force increases further and the strands align more with the force, the curves cross (at ≈ 5 pN), and poly(dA) becomes less extensible because of its shorter effective contour length.

Increasing the force also leads to significant changes in the average length of stacked regions in poly(dA). Interestingly, at low force, the lower entropic cost for aligning longer stacked sections leads to an initial increase in $\langle P_{st} \rangle$ and $\langle l \rangle$ with force (up to around 5 pN). However, as the force increases further, both $\langle P_{st} \rangle$ and $\langle l \rangle$ start to decrease because it becomes favorable for the strand to disrupt stacking to allow for greater extension. The reduction in stacking is particularly significant for the poly(dA) strand over the range 15 to 25 pN, the location of the concave region in the force-extension curve. The long stacked regions are broken down into shorter ones, which facilitates an increase in the overall length of the polymer. However, a short region of 3 bases can still align its backbone with the force while remaining stacked, as illustrated in Fig. 7(f). Therefore, even though it is progressively reduced with force for both poly(dA) and poly(dGdA), a significant degree of stacking is preserved even at high forces.

The changes in stacking hence explain the physical cause of the concave “plateau” region in the force-extension curve for the stronger-stacking strand, poly(dA). It corresponds to the structural transition as the increasing force disrupts the long stacked regions and $\langle l \rangle$ decreases. The concave segment of the force-extension curve is not present for poly(dGdA) because the latter already consists of mostly short stacked regions at zero force.

The differences in the structure of the poly(dA) and poly(dGdA) strands described above are further illustrated in Figs. 7(d) and 7(e), where snapshots of the sequences are shown for a force of 15 pN. The poly(dA) strands are clearly much more stacked than the poly(dGdA) strands are, and also

more strongly aligned with the force. From this picture, one can also see why the derivative of the force-extension curve begins to rise steeply for the poly(dA) curve around 15 pN: the highly stacked strand is nearing its maximum extension, whereas the unstacked strand is not.

It is interesting to note that a mere 20% difference in stacking probability between poly(dA) and poly(dGdA) at zero force causes a significant difference in the average length of stacked regions: $\langle l \rangle \cong 8$ versus $\langle l \rangle \cong 2$. This effect can be understood by considering a simple, uncooperative model for stacking along the strand. Let p be the probability that two neighbors are stacked and $P(l)$ the probability that a stacked cluster has length l . Assuming an infinitely long polymer chain, the probability of having a continuously stacked region of length l is $P(l) = (1 - p)p^l$, which is the probability of having l subsequent base pairs stacked (each with probability p) and the $(l + 1)$ th base not stacked with the next base along the chain (which is with probability $1 - p$). The average length $\langle l \rangle_{\text{uncoop}}$ of a stacked region in this uncooperative model can thus be obtained by summing over l

$$\langle l \rangle_{\text{uncoop}} = \sum_{l=0}^{\infty} l P(l) = \frac{p}{1 - p}. \quad (11)$$

Since our model has low stacking cooperativity,³⁵ we can make the approximation $p \approx \langle P_{\text{st}} \rangle$. Figure 7(c) shows that this simple model compares remarkably well with the measured values of $\langle l \rangle$. The fact that $\langle l \rangle$ diverges as $\langle P_{\text{st}} \rangle$ approaches 1 explains the sensitivity of the model strands to relatively small changes in stacking propensity at large $\langle P_{\text{st}} \rangle$ and also explains the large differences in $\langle l \rangle$ observed at zero force.

It is illuminating to compare our results to the theoretical model used by Seol *et al.* in Ref. 73 to explain the observed force-extension curves of RNA. Their model makes similar physical assumptions to the behavior of our coarse-grained model: the single strand is split into rigid helical regions and flexible random coil regions. Thus, the basic explanation for the plateau region is the same as in our model. However, there are also some differences. For example, our model suggests that absence of a plateau in the force extension curve does not necessarily mean the absence of stacking. In fact, we have observed that short stacked regions persist even while pulling the strand at a high force, because our model allows for three bases to remain stacked while aligning the backbone with the applied force, a feature that is not present in the model used in Ref. 73. Moreover, the concave region in the force-extension curve interpreted with our model would indicate the presence of a much stronger stacking propensity than the one derived in Ref. 73. Although our description of single strands is fairly simple, it incorporates the underlying physics of the model of Ref. 73 and in addition provides an explicit 3-dimensional representation of single-stranded nucleic acids. In summary, we believe that the presence of concave region in the force extension curve suggests that long stacked regions are present in the relaxed strand. This would either indicate strong uncooperative stacking, as in our model, or large cooperativity in stacking.

E. The structure of a kissing complex

In a recent publication,³⁷ we investigated DNA kissing complexes, a system where topological and geometrical frustration have important effects, and studied the ability of the original average base model to describe these systems. In this section, we show how the sequence dependence of interactions can introduce non-trivial changes to the structure of a kissing complex, with potential importance for the operation of nanotechnological systems.⁸⁰⁻⁸⁵

A kissing complex is a system in which two hairpins have loop regions that are complementary and can thus at least partially hybridize (see Fig. 8(a)). They are a common motif in RNA and are expected to form in DNA nanotechnology systems where complementary hairpins are used as fuel for DNA nanomachines.^{80,86} In the experimental system realized in Ref. 80, two strands of 40 nucleotides were designed to be both complementary and also able to form a hairpin with a stem of 10 base pairs. As the remaining 20-base loops are complementary to each other, the two hairpins can form a kissing complex. The sequences are⁸⁰

```
3'-CGCAACGACG-GCTCCCCTCTTCTCATTTTA-
CGTCGTTGCG-5'
and
3'-CGCAACGACG-TAAAATGAGAAGAGGGGAGC-
CGTCGTTGCG-5',
```

where the hyphens separate stem and loop regions. A dilute solution of such strands tends to form hairpins much more quickly than full duplexes, due to a lower kinetic barrier for the former process. The hairpins in turn form kissing complexes, an intermediate metastable state with respect to full hybridization that requires a significant amount of rearrangement to transform into the full duplex. The kinetic barrier, due to the topological frustration of the complex, is so high that full hybridization is almost impossible. However, this barrier can be reliably resolved by the introduction of a DNA catalyst strand, designed to open one of the hairpins by displacement and trigger full hybridization, thus releasing the stored free-energy.⁸⁰

Following Ref. 80, we studied in Ref. 37 the structure of the resulting kissing complex with the average sequence parametrization. We found that the system typically assumed a structure with two symmetric parallel helices, as shown in Fig. 8(a). However, as the loop sequences used in Ref. 80 are very asymmetric in G-C content, we expect that the average parametrization should overestimate the stability of the weakly bound region and conversely underestimate that of the strongly bound, G-C-rich region.

When we repeated the structural study with the sequence-dependent potential, we obtained a qualitatively different result. Computing the binding free-energy profile of the system, using the number of native base pairs (i.e., base pairs that would be present in the final full duplex) as a reaction coordinate (Fig. 8(c)), we found a second minimum at around nine interstrand base pairs that was not observed for the average parametrization. A typical configuration associated with this minimum is shown in Fig. 8(b). It is evident that as well as being able to form the structure with two symmetric helices, the system is also able to adopt an alternative structure with

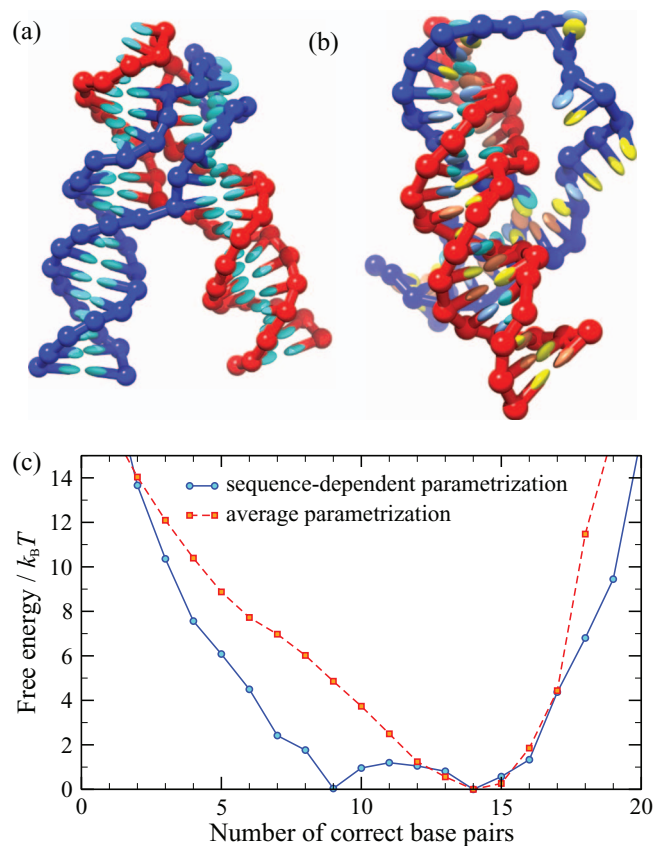


FIG. 8. Effects of sequence dependence on the structure of kissing hairpins. (a) Typical structure found in both the average and sequence-dependent parametrization, with 14 intramolecular base pairs. (b) Second free energy minimum found only in the sequence-dependent parametrization, with 9 intramolecular base pairs. Please note the exposed bases—not present in (a)—that can be used as a toehold by the catalyst strand to initiate displacement. (c) Free energy profile for binding with the two parametrizations, with the sequence-dependent one exhibiting a second minimum corresponding to the structure depicted in (b).

a single intermolecular helix that both contains the G-C-rich section and is slightly larger than either individual helix in the two-helix form.

This competing minimum has potentially important consequences for the nanotechnological applications of kissing hairpins. In Ref. 80, a catalyst strand was introduced to the system in order to facilitate full hybridization of the complex: the strand was designed to bind to the weaker half of one of the loops, and then to open up the hairpin by displacement. The fact that a competing minimum exists in which the whole weaker half of the loop is available for binding will favor this process, as it provides a long, easily accessible toehold for displacement. Such toeholds are known⁷¹ to accelerate displacement reactions by several orders of magnitude. Our model suggests that if the strand was instead designed to bind to the stronger half of the loop, its effectiveness would be hindered rather than helped by the presence of the alternative minimum. We would therefore expect such a catalyst to be less effective than the one used in Ref. 80.

The qualitative difference between the results of the two parametrizations in this case highlights that if one is interested in the detailed properties of a system like this one, where short binding regions with asymmetric G-C content are present, it is

important to have a model with sequence-dependent binding strengths to be able to make more accurate predictions. Were the G-C pairs in the loop more evenly distributed, we would expect the results of the average parametrization free energy profile to accurately describe the kissing complex.

VI. CONCLUSIONS

We have extended the nucleotide-level coarse-grained DNA model of Ouldrige *et al.*³⁵ (which distinguishes between A-T and G-C base-pairing but otherwise treats these interactions at the average base level) to include sequence-dependent stacking and hydrogen-bonding interactions. To derive the new parameters, we developed a histogram reweighting procedure that allowed us to fit to thousands of melting temperatures of oligomers ranging in length from 6 to 18 base pairs. Melting temperatures were extracted from SantaLucia's nearest-neighbor model,⁴⁷ which we treat here as a good fit to experiment.

Sequence can have an important effect on melting temperatures. For the same length oligomer, but different sequences, melting temperatures can differ by as much as 50 °C. Even for the same sequence content, but different base-pair ordering, variations in stacking energies mean that melting temperatures can vary by up to 12 °C. Our new parametrization reproduces these differences and on average agrees to within a standard deviation of 0.85 °C with the SL nearest-neighbor model. In contrast to the model's ability to capture thermodynamic properties, our coarse-grained model does not attempt to include the effects of sequence on structural or mechanical properties of double-stranded DNA. Instead, these remain as previously reported in Ref. 35.

Our new thermodynamic parametrization opens up the possibility of investigating sequence-dependent DNA phenomena. Specifically, we have considered here the following five systems:

(a) *Heterogeneous stacking transition in single-stranded DNA:* Even though our stacking parameters do not vary by more than 7%, they can induce significant spatial and temporal heterogeneity in the stacking of single strands. For example, the difference in stacking probability between the strongest and the weakest stacking pairs in the oligomer we studied is large enough that the midpoints of the stacking transition of two distinct pairs in a single strand can be separated by as much as 40 °C. These results suggest that structural and mechanical properties of single-stranded DNA should be highly heterogeneous as well.

(b) *The hybridization free energy profiles of duplexes:* We studied three different 12mer sequences at their respective melting temperatures, finding that sequence heterogeneity also has significant effects on the probability that the ends of a duplex are open, i.e., that they fray. We found that A-T ends are typically frayed, while sequences with G-C ends exhibit a free-energy minimum for a completely closed duplex.

(c) *The effect of stacking strength in the loop on hairpin stability:* The SL model only distinguishes base-pair steps. Given that we used this model to generate the melting temperatures to which we fit, we were unable to uniquely isolate the stacking strength of individual base combinations.

Additional experimental data on single-stranded stacking are needed to separate these interactions. One potential source of data that goes beyond the SL model is given by experiments on melting of hairpins with poly(dA) and poly(dT) loops.⁷² By calculating how increasing the stacking strength in the loop lowers the melting temperatures, we showed that parameters could be derived that reproduce the expected stronger AA compared to TT stacking, without significantly changing the quality of our fit to the overall melting temperatures of duplexes. Nevertheless, we do not yet include this difference in our parametrization, because to be consistent we would need similar data to distinguish between other base-pair steps.

(d) The force-extension properties of single strands:

Another experimental situation where differences in single-stranded stacking have been measured experimentally is in the force extension of ssDNA. We show that more strongly stacked sequences should be more extensible for small forces up to about 5 pN. For certain sequences, experiments have observed a concave “plateau” region in the force-extension curves. We are able to qualitatively reproduce this feature and, in agreement with previous explanations,⁷³ attribute the plateau region to the different force response of stiffer stacked and more flexible unstacked regions. Furthermore, we show that the onset of the plateau region is correlated with a sharp decrease in the average length of stacked regions with increasing force. Because the average length of stacked regions drops rapidly with a relatively small decrease in the average stacking, we argue that a very large propensity to stack (>90%) is necessary to give a similar results to those observed in experiment. We therefore conclude that if these phenomena are to be explained through largely uncooperative stacking of bases to form helical ssDNA, as in our model, a high stacking propensity is required. Furthermore, failure to observe a force plateau for a sequence does not imply an absence of significant stacking.

(e) The structure of a kissing-loop complex: Finally, we applied our model to study the effect of sequence on the structure of a kissing complex formed by two hairpins. When the sequences used in the experiments of Ref. 80 are studied, the average base model exhibits one minimum free-energy structure,³⁷ while our sequence-dependent model also generates a second, qualitatively distinct, stable structure. The new structure completely exposes a toehold, which may significantly accelerate the DNA catalyst mediated release of free energy stored in the kissing complex.

The examples described above suggest that our model can be used for many other DNA applications in nanotechnology and biology where sequence plays a significant role. Our model should work particularly well for situations where single-to-double stranded transitions are important. Nevertheless, users of our model should remain aware of some limitations. First, the model is only fit to a single salt concentration of $[Na^+] = 0.5$ M, where the electrostatic properties are strongly screened. A new kind of parametrization may be necessary to reach significantly lower salt concentrations. Second, the model lacks certain detailed local structural information, such as major and minor grooving, or sequence dependent elastic parameters. Furthermore, our model was fit to data that only includes the effects of base-pair steps. New

experimental results on single-stranded stacking are needed to separate out the stacking strength of individual base combinations. Applications where the effects we neglect are crucial may therefore be best studied by other models.

We are developing further improvements to the model, but our work also highlights the need for new systematic experiments, in particular to elucidate the basic physics of single-stranded stacking interactions. Such information would be also of great help to those studying DNA-coated colloids.⁸⁷

To summarize, we have introduced a new coarse-grained model of DNA that has been parametrized to reproduce the thermodynamic effects of sequence-dependent interactions. The current version of the model provides a computationally efficient and physically accurate tool for the study of problems ranging from DNA nanotechnology to biology. To facilitate its use, we have made simulation code implementing Monte Carlo and Brownian dynamics for the model available as a free software called oxDNA at <http://dna.physics.ox.ac.uk>.

ACKNOWLEDGMENTS

The authors would like to thank Erik Winfree, Filip Lankaš, Felix Ritort, and Agnes Noy for helpful discussions. The authors also acknowledge financial support from the Engineering and Physical Sciences Research Council, University College (Oxford), and from the Oxford Supercomputing Centre for computer time. P.Š. is grateful for the award of a Scatcherd European Scholarship.

¹W. Saenger, *Principles of Nucleic Acid Structure* (Springer-Verlag, New York, 1984).

²L. Adleman, *Science* **266**, 1021 (1994).

³J. Bath, S. J. Green, and A. J. Turberfield, *Angew. Chem., Int. Ed.* **117**, 4432 (2005).

⁴J. Bath, S. J. Green, K. E. Allan, and A. J. Turberfield, *Small* **5**, 1513 (2009).

⁵E. Winfree, F. R. Liu, L. A. Wenzler, and N. C. Seeman, *Nature (London)* **394**, 539 (1998).

⁶P. W. K. Rothmund, *Nature (London)* **440**, 297 (2006).

⁷J. Šponer, K. E. Riley, and P. Hobza, *Phys. Chem. Chem. Phys.* **10**, 2595 (2008).

⁸A. Pérez, A. Noy, F. Lankaš, F. J. Luque, and M. Orozco, *Nucleic Acids Res.* **32**, 6144 (2004).

⁹P. Hobza and J. Šponer, *Chem. Rev.* **99**, 3247 (1999).

¹⁰J. Šponer *et al.*, *Chem.-Eur. J.* **12**, 2854 (2006).

¹¹D. Svozil, P. Hobza, and J. Šponer, *J. Phys. Chem. B* **114**, 1191 (2010).

¹²J. Šponer, P. Jurečka, and P. Hobza, *J. Am. Chem. Soc.* **126**, 10142 (2004).

¹³W. D. Cornell *et al.*, *J. Am. Chem. Soc.* **117**, 5179 (1995).

¹⁴B. R. Brooks *et al.*, *J. Comput. Chem.* **4**, 187 (1983).

¹⁵A. Pérez, F. J. Luque, and M. Orozco, *Acc. Chem. Res.* **45**, 196 (2012).

¹⁶E. J. Sambriski, D. C. Schwartz, and J. J. de Pablo, *Biophys. J.* **96**, 1675 (2009).

¹⁷J. C. Araque, A. Z. Panagiotopoulos, and M. A. Robert, *J. Chem. Phys.* **134**, 165103 (2011).

¹⁸M. C. Linak, R. Tourdot, and K. D. Dorfman, *J. Chem. Phys.* **135**, 205102 (2011).

¹⁹K. Drukker, G. Wu, and G. C. Schatz, *J. Chem. Phys.* **114**, 579 (2001).

²⁰M. Sales-Pardo, R. Guimera, A. A. Moreira, J. Widom, and L. Amaral, *Phys. Rev. E* **71**, 051902 (2005).

²¹M. Kenward and K. D. Dorfman, *J. Chem. Phys.* **130**, 095101 (2009).

²²T. E. Ouldridge, I. G. Johnston, A. A. Louis, and J. P. K. Doye, *J. Chem. Phys.* **130**, 065101 (2009).

²³T. A. Knotts IV, N. Rathore, D. C. Schwartz, and J. J. de Pablo, *J. Chem. Phys.* **126**, 084901 (2007).

- ²⁴A.-M. Florescu and M. Joyeux, *J. Chem. Phys.* **135**, 085105 (2011).
- ²⁵A. Morriss-Andrews, J. Rottler, and S. S. Plotkin, *J. Chem. Phys.* **132**, 035105 (2010).
- ²⁶A. V. Savin, M. A. Mazo, I. P. Kikot, L. I. Manevitch, and A. V. Onufriev, *Phys. Rev. B* **83**, 245406 (2011).
- ²⁷P. D. Dans, A. Zeida, M. R. Machado, and S. Pantano, *J. Chem. Theory Comput.* **6**, 1711 (2010).
- ²⁸A. Saveliev and G. A. Papoian, *Biophys. J.* **96**, 4044 (2009).
- ²⁹N. B. Becker and R. Everaers, *Phys. Rev. E* **76**, 021923 (2007).
- ³⁰F. Lankaš, *Innovations in Biomolecular Modeling and Simulations*, RSC Biomolecular Sciences Vol. 2 (The Royal Society of Chemistry, 2012).
- ³¹T. Dauxois, M. Peyrard, and A. R. Bishop, *Phys. Rev. E* **47**, 684 (1993).
- ³²C. Nisoli and A. R. Bishop, *Phys. Rev. Lett.* **107**, 068102 (2011).
- ³³S. Cocco and R. Monasson, *Phys. Rev. Lett.* **83**, 5178 (1999).
- ³⁴T. E. Ouldridge, A. A. Louis, and J. P. K. Doye, *Phys. Rev. Lett.* **104**, 178101 (2010).
- ³⁵T. E. Ouldridge, A. A. Louis, and J. P. K. Doye, *J. Chem. Phys.* **134**, 085101 (2011).
- ³⁶T. E. Ouldridge, "Coarse-grained modelling of DNA and DNA nanotechnology," D.Phil. dissertation (University of Oxford, 2011), available at <http://tinyurl.com/7ycbx7c>.
- ³⁷F. Romano, A. Hudson, J. P. K. Doye, T. E. Ouldridge, and A. A. Louis, *J. Chem. Phys.* **136**, 215102 (2012).
- ³⁸C. De Michele, L. Rovigatti, T. Bellini, and F. Sciortino, *Soft Matter* **8**, 8388 (2012).
- ³⁹C. Matek, T. E. Ouldridge, A. Levy, J. P. K. Doye, and A. A. Louis, "DNA Cruciform Arms Nucleate through a Correlated but Asynchronous Cooperative Mechanism," *J. Phys. Chem. B* (to be published).
- ⁴⁰C. Calladine and H. Drew, *Understanding DNA: The Molecule and How It Works* (Academic, 1997).
- ⁴¹W. K. Olson, A. A. Gorin, X.-J. Lu, L. M. Hock, and V. B. Zhurkin, *Proc. Natl. Acad. Sci. U.S.A.* **95**, 11163 (1998).
- ⁴²S. Geggier and A. Vologodskii, *Proc. Natl. Acad. Sci. U.S.A.* **107**, 15421 (2010).
- ⁴³B. Basham, G. P. Schroth, and P. S. Ho, *Proc. Natl. Acad. Sci. U.S.A.* **92**, 6464 (1995).
- ⁴⁴We use poly-dC,dA,dT, and dG notation for DNA sequences with repeated nucleotide content to distinguish them from RNA sequences, which are referred to with rC, rA, rU, and rG.
- ⁴⁵B. Alberts *et al.*, *Molecular Biology of the Cell*, 4th ed. (Garland Science, 2002).
- ⁴⁶V. Ortiz and J. J. de Pablo, *Phys. Rev. Lett.* **106**, 238107 (2011).
- ⁴⁷J. SantaLucia, Jr., *Proc. Natl. Acad. Sci. U.S.A.* **17**, 1460 (1998).
- ⁴⁸J. SantaLucia, Jr. and D. Hicks, *Annu. Rev. Biophys. Biomol. Struct.* **33**, 415 (2004).
- ⁴⁹J. N. Zadeh *et al.*, *J. Comput. Chem.* **32**, 170 (2011).
- ⁵⁰N. R. Markham and M. Zuker, *Methods Mol. Bio.* **453**, 3 (2008).
- ⁵¹N. R. Markham and M. Zuker, *Nucleic Acids Res.* **33**, W577 (2005).
- ⁵²N. L. Novere, *Bioinformatics* **17**, 1226 (2001).
- ⁵³B. H. Zimm, *J. Chem. Phys.* **33**, 1349 (1960).
- ⁵⁴D. Poland and H. A. Scheraga, *J. Chem. Phys.* **45**, 1464 (1966).
- ⁵⁵D. Poland and H. A. Scheraga, *Theory of Helix-Coil Transitions in Biopolymers: Statistical Mechanical Theory of Order-disorder Transitions in Biological Macromolecules* (Academic, New York, 1970).
- ⁵⁶D. Jost and R. Everaers, *Biophys. J.* **96**, 1056 (2009).
- ⁵⁷A. Krueger, E. Protozanova, and M. D. Frank-Kamenetskii, *Biophys. J.* **90**, 3091 (2006).
- ⁵⁸T. Ambjörnsson, S. K. Banik, O. Krichevsky, and R. Metzler, *Phys. Rev. Lett.* **97**, 128105 (2006).
- ⁵⁹T. Ambjörnsson, S. K. Banik, O. Krichevsky, and R. Metzler, *Biophys. J.* **92**, 2674 (2007).
- ⁶⁰J. M. Huguet *et al.*, *Proc. Natl. Acad. Sci. U.S.A.* **107**, 15431 (2010).
- ⁶¹T. E. Ouldridge, A. A. Louis, and J. P. K. Doye, *J. Phys.: Condens. Matter* **22**, 104102 (2010).
- ⁶²A. M. Ferrenberg and R. H. Swendsen, *Phys. Rev. Lett.* **61**, 2635 (1988).
- ⁶³D. Landau and K. Binder, *A Guide to Monte Carlo Simulations in Statistical Physics* (Cambridge University Press, New York, NY, 2005).
- ⁶⁴G. Torrie and J. P. Valleau, *J. Comp. Phys.* **23**, 187 (1977).
- ⁶⁵W.-S. Chen *et al.*, *Phys. Rev. Lett.* **105**, 218104 (2010).
- ⁶⁶S. Whitelam, E. H. Feng, M. F. Hagan, and P. L. Geissler, *Soft Matter* **5**, 1521 (2009).
- ⁶⁷D. Frenkel and B. Smit, *Understanding Molecular Simulation: From Algorithms to Applications*, 1st ed. (Academic, Orlando, FL, 1996).
- ⁶⁸J. Russo, P. Tartaglia, and F. Sciortino, *J. Chem. Phys.* **131**, 014504 (2009).
- ⁶⁹J. Holbrook, M. Capp, R. Saecker, and M. Record, *Biochemistry* **38**, 8409 (1999).
- ⁷⁰S. Nonin, J.-L. Leroy, and M. Gueron, *Biochemistry* **34**, 10652 (1995).
- ⁷¹D. Y. Zhang and E. Winfree, *J. Am. Chem. Soc.* **131**, 17303 (2009).
- ⁷²N. L. Goddard, G. Bonnet, O. Krichevsky, and A. Libchaber, *Phys. Rev. Lett.* **85**, 2400 (2000).
- ⁷³Y. Seol, G. M. Skinner, K. Visscher, A. Buhot, and A. Halperin, *Phys. Rev. Lett.* **98**, 158103 (2007).
- ⁷⁴Y. Seol, G. M. Skinner, and K. Visscher, *Phys. Rev. Lett.* **93**, 118102 (2004).
- ⁷⁵G. Mishra, D. Giri, and S. Kumar, *Phys. Rev. E* **79**, 031930 (2009).
- ⁷⁶M.-N. Dessinges *et al.*, *Phys. Rev. Lett.* **89**, 248102 (2002).
- ⁷⁷S. B. Smith, Y. Cui, and C. Bustamante, *Science* **271**, 795 (1996).
- ⁷⁸Y. Zhang, H. Zhou, and Z.-C. Ou-Yang, *Biophys. J.* **81**, 1133 (2001).
- ⁷⁹A. Montanari and M. Mézard, *Phys. Rev. Lett.* **86**, 2178 (2001).
- ⁸⁰J. Bois *et al.*, *Nucleic Acids Res.* **33**, 4090 (2005).
- ⁸¹R. M. Dirks and N. A. Pierce, *Proc. Natl. Acad. Sci. U.S.A.* **101**, 15275 (2004).
- ⁸²S. Venkataraman, R. M. Dirks, P. W. K. Rothmund, E. Winfree, and N. A. Pierce, *Nat. Nanotechnol.* **2**, 490 (2007).
- ⁸³S. J. Green, J. Bath, and A. J. Turberfield, *Phys. Rev. Lett.* **101**, 238101 (2008).
- ⁸⁴P. Yin, H. M. Choi, C. R. Calvert, and N. A. Pierce, *Nature (London)* **451**, 318 (2008).
- ⁸⁵R. A. Muscat, J. Bath, and A. J. Turberfield, *Nano Lett.* **11**, 982 (2011).
- ⁸⁶S. J. Green, D. Lubrich, and A. J. Turberfield, *Biophys. J.* **91**, 2966 (2006).
- ⁸⁷B. M. Mladek, J. Fornleitner, F. J. Martinez-Veracochea, A. Dawid, and D. Frenkel, *Phys. Rev. Lett.* **108**, 268301 (2012).